Event-Triggered Robust Path Tracking Control Considering Roll Stability Under Network-Induced Delays for Autonomous Vehicles

Fernando Viadero-Monasterio, Anh-Tu Nguyen, *Senior Member, IEEE*, Jimmy Lauber, Maria Jesus L. Boada, and Beatriz L. Boada

***Abstract*— This paper proposes a multi-input multi-output (MIMO) method for path tracking control of autonomous vehicles under network-induced delays while taking into account the roll dynamics to improve both the driving safety and the passenger comfort. The steering control is directly applied to the front wheels, while the anti-roll moment is exerted by an active suspension. The asynchronous phenomenon caused by the sampling process and the time-varying vehicle speed are explicitly taken into account in the control design using a polytopic linear parameter-varying (LPV) control approach. Moreover, to avoid using costly vehicle sensors and complex control structures, a static output feedback (SOF) control scheme is considered. An effective event-triggering mechanism is also proposed to alleviate the communication burden of the vehicle networked control system. Based on augmented Lyapunov-Krasovskii functional, the control design conditions are derived to guarantee the vehicle closed-loop stability under the effects of transmission delays, event-triggered control signals and time-varying parameters. The design procedure is reformulated as an iterative optimization problem involving linear matrix inequality (LMI) constraints, which can be effectively solved with available numerical solvers. The proposed event-triggered SOF controller is evaluated with the vehicle dynamics simulation software CarSim under several dynamic scenarios. A comparative study with related vehicle control results is performance to emphasize the effectiveness of the control method in terms of path tracking performance, driving safety and comfort, and data communication efficiency of the vehicle networked control system.**

***Index Terms*— Path tracking, active suspension, roll stability control, networked control systems, event-triggered control.**

Manuscript received 13 December 2022; revised 30 May 2023 and 25 August 2023; accepted 28 September 2023. Date of publication 13 October 2023; date of current version 29 November 2023. This work was supported in part by the National Funding and Cooperation—Research and Development Projects (RDPs) under Grant PID2022-136468OB-I00, in part by the Recherche et Innovation en Transports et Mobilité Eco-responsables et Autonomes (RITMEA) Program of the Hauts-de-France Region, in part by the European Community, in part by the Regional Delegation for Research and Technology, in part by the French Ministry of Higher Education and Research, and in part by the French National Center for Scientific Research. The Associate Editor for this article was Z. Liu. *(Corresponding author: Fernando Viadero-Monasterio.)*

Fernando Viadero-Monasterio is with Department of Mechanical Engineering, University Carlos III de Madrid, Leganes, 28911 Madrid, Spain, and also with the LAMIH, CNRS, UMR 8201, Université Polytechnique Hauts-de-France, 59313 Valenciennes, France (e-mail: fviadero@ing.uc3m.es).

Anh-Tu Nguyen and Jimmy Lauber are with the LAMIH, CNRS, UMR 8201, Université Polytechnique Hauts-de-France, 59313 Valenciennes, France, and also with the INSA Hauts-de-France, 59313 Valenciennes, France (e-mail: tnguyen@uphf.fr; jlauber@uphf.fr).

Maria Jesus L. Boada and Beatriz L. Boada are with the Department of Mechanical Engineering, University Carlos III de Madrid, Leganes, 28911 Madrid, Spain (e-mail: mjboada@ing.uc3m.es; bboada@ing.uc3m.es).

Digital Object Identifier 10.1109/TITS.2023.3321415

I. Introduction

DEVELOPING automated driving systems has attracted a considerable interest from both industry and academia due to their great contribution to reduce traffic accidents, increase mobility, and to mitigate environmental pollution. One of the most important automated driving tasks is the path tracking [1], [2], [3], which must guarantee not only the safety but also the comfort of the autonomous vehicles.

Passengers in a rollover accident are 10 times more likely to die than on a non-rollover accident [4]. This kind of situations implies 33% of all passenger car crashes [5]. Recently, sport utility vehicles have become a growing trend. These vehicles are more prone to rollover accidents because of their high center of mass position with a narrow wheelbase [6], [7]. Due to the aforementioned reasons, researchers have focused on the vehicle roll stability control (RSC). Some of the existing control methods are based on active steering control [8], differential braking control [9], active stabilizer bar control [10], or suspension control [11]. Although these works present a possible solution to avoid rollover, they do not consider the lateral dynamics nor the path tracking problem. Since the roll dynamics and the lateral dynamics are highly coupled, it is challenging to achieve an adequate tradeoff between these dynamics. Moreover, if the vehicle deviates from the desired trajectory, it might impact on other vehicles, which can cause new accidents. Hence, it is crucial to focus on path tracking performance while improving the roll stability. Path tracking control is concerned with designing a steering control law to guide the vehicle to follow a desired trajectory, defined by a vehicle path planner [12], [13].

The path tracking control of autonomous vehicles has been widely studied in the literature. Zhou et al. [14] proposed a Popov-$\mathscr{H}_\infty$ robust path tracking control method while taking into account the sector-bounded kinematic nonlinearity. In [15], a robust gain-scheduling energy-to-peak control of vehicle lateral dynamics was proposed. Alcala et al. [16] developed a Lyapunov-based control technique with an LQR-LMI tuning method for autonomous vehicles, where a kinematics vehicle model was considered. However, none of these works analyzed the vehicle roll behavior while designing path tracking controllers. A model predictive control (MPC) method was applied for path tracking considering the rollover stability in [17], where the front-wheel steering and the external yaw

moment are used as control inputs. An MPC controller was considered in [18] for path tracking control, where a fuzzy PID controller was used to ensure the roll stability by controlling the braking force on each tire. However, due to the complex nature of the vehicle models used for control design, most of existing results separately consider the roll control and the path tracking control without guaranteeing a global vehicle stability, *i.e.*, single-input single-output (SISO) control approaches. MPC techniques have shown large potential for vehicle control [19]. However, when the vehicle control system becomes highly nonlinear and uncertain, linear MPC technique may not be effective due to the lack of robustness performance. Moreover, some major challenges remain when using robust/nonlinear MPC techniques [3], [19]. First, MPC control can require a costly calibration effort in many cases. Second, the nonlinear MPC control design is still too computationally complex. Third, guaranteeing the stability of MPC *a priori*, without increasing excessively the algorithm complexity is still widely open. Linear parameter-varying (LPV) control technique could be an effective alternative to overcome these major drawbacks for complex vehicle systems [3]. A robust $\mathscr{H}_\infty$ dynamic output feedback controller was designed in [20] to follow predefined paths. In [10], the roll behavior was enhanced through an active stabilizer bar, whose anti-roll moment is controlled by a two-input fuzzy controller. Note that using active stabilizer bars can significantly increase the energy consumption. Moreover, they can often exert only a tight maximum anti-roll moment. An adaptive fuzzy controller was designed in [21] for active suspension systems to enhance the vertical and roll chassis motions. However, based on a fuzzy logic control scheme, the vehicle closed-loop stability cannot be guaranteed.

In networked control systems (NCSs), the information of the plant is sampled and sent to different nodes [22]. In autonomous vehicles, control area network (CAN) is commonly utilized for in-vehicle communication due to its robustness and lightweight properties [23]. If the sampling frequency is high, the amount of data transmitted between the different elements can become large. This may imply that the network communication is not enough efficient, as the information does not significantly differ between consecutive data packets. As a result, communication delays may increase. To deal with communication delays, a trajectory tracking MPC method considering a random network delay is introduced in [24]. However, the computational time required for the online MPC optimization does not satisfy the real-time requirements. A robust $\mathscr{H}_\infty$ path following control strategy for autonomous vehicles with delays was presented in [25]. The authors in [26] proposed a robust gain-scheduling control method for autonomous path following systems with stochastic network-induced delay. However, the above-mentioned works assume that all the vehicle states are measurable. Moreover, these works do not consider the roll dynamics for control design. To reduce the amount of data transmitted over time, and to avoid saturating the communication network, event-triggered controllers can be designed to discard the transmission of data packets that do not include relevant control information [27], [28], [29], [30], [31], [32]. Hence, any possible saturation of the vehicle control network can be avoided. Event-triggered control has been widely considered in several areas, leading to different event-triggering rules. If the involved processing data is continuous, then the design of an event-triggering mechanism has to achieve Zeno-freeness. To this end, the authors in [28] defined two different thresholds for the event-triggering condition, one proportional and another additive to the value of the previous data transmitted. In [29], an integral-based event-triggered scheme was established. However, a fixed waiting time is defined to avoid Zeno behavior. When signals to transmit are previously sampled, as they might be obtained from sensors or data-loggers with prescribed data acquisition rate, Zeno behavior does not occur and the closed-loop stability analysis can be simplified, as the event-triggering mechanism is periodically executed [30], [31], [32]. Zhang et al. [33], the authors focused on the control of an active suspension to improve ride comfort and safety. An observer-based decentralized event-triggered control scheme is defined. Nevertheless, network-induced transmission delays are not taken into account.

Motivated by the above vehicle control issues, this paper proposes a new multi-input multi-output (MIMO) linear parameter varying (LPV) controller for path tracking control of autonomous vehicles while taking into account the roll dynamics and network-induced delays. The path tracking control is performed by acting on the steering wheel, while the roll stability control can be achieved via an active suspension. Based on a static output feedback (SOF) control scheme, the control signals can be computed using solely sensors installed in series-production vehicles. A periodic event-triggering mechanism is defined to reduce the amount of control orders sent to the steering system and the active suspension system. To take into account the network-induced delay in the control design, an augmented Lyapunov-Krasovskii functional is used to derive the design conditions, which satisfy some predefined closed-loop specifications. The LPV control design procedure is expressed in terms of an iterative linear matrix inequality (LMI) optimization, which can be effectively solved with semidefinite programming techniques. Specifically, the main contributions can be summarized as follows.

- We propose a new MIMO approach for combined path tracking and roll stability control of autonomous vehicles to take into account not only the driving safety but also the passenger comfort.
- A polytopic SOF control scheme is leveraged to deal with the unavailability of full-state vehicle information due to the sensor cost issues while avoiding additional observers or complex dynamic control schemes.
- The in-vehicle communication delay and the asynchronous phenomenon caused by the sampling process are explicitly taken into account in the control design via a polytopic LPV approach together with Lyapunov-Krasovskii stability theory.
- A new event-triggering mechanism is proposed to reduce the data exchange burden of the vehicle control system.

TABLE I
VEHICLE PARAMETERS

Parameter	Value	Description
l_f	$1.42\ m$	Distance of the front axle from the center of gravity (CoG)
l_r	$0.85\ m$	Distance of the rear axle from CoG
t_f	$0.78\ m$	Half vehicle track, front axle
t_r	$0.75\ m$	Half vehicle track, rear axle
K_ϕ	$31752\ Nm/rad$	Roll stiffness coefficient
C_ϕ	$7025.4\ Nms/rad$	Roll damping coefficient
$C_{\alpha f}$	$30000\ N/rad$	Cornering stiffness of the front tire
$C_{\alpha r}$	$25000\ N/rad$	Cornering stiffness of the rear tire
g	$9.81\ m/s^2$	Acceleration of gravity
h_{cr}	$0.35\ m$	Distance from roll center to CoG
I_x	$520\ kgm^2$	Moment of inertia about the roll axis
I_z	$1110.9\ kgm^2$	Moment of inertia about the yaw axis
M	$650\ kg$	Vehicle mass

The proposed event-triggered SOF control method is validated with the vehicle dynamics simulation software CarSim under different challenging scenarios. A comparative study is performed to highlight the effectiveness of the new method with respect to state-of-the-art vehicle control results.

Notation. The set of nonnegative integers is denoted by $\mathbb{Z}_+$. For a matrix X, $X^\top$ denotes its transpose. If Y is a square matrix, $Y > 0$ means that Y is positive definite. In a symmetric matrix, the symbol $*$ denotes the transpose of the symmetric term. The function $\mathrm{He}\{Y\} = Y + Y^\top$. $\mathrm{diag}(X_1, X_2)$ denotes a block-diagonal matrix composed of X_1 and X_2. For a scalar x, $\overline{x}$ and $\underline{x}$ are respectively the maximum and minimum values of x. Arguments are omitted when their meaning is clear.

II. VEHICLE MODELING AND PROBLEM FORMULATION

This section first presents the vehicle modeling for control purposes. Then, the control problem of interest is formulated.

A. Vehicle Modeling

For path tracking control design, we consider both lateral and roll dynamics as depicted in Fig. 1. The vehicle parameters are given in Table I. This vehicle model has three degrees of freedom, *i.e.*, the sideslip angle β, the yaw rate r, and the roll angle ϕ. The vehicle dynamics can be described as [34]

$$\begin{aligned}
\dot\beta &= -\frac{I_{eq}\left(C_{\alpha f}+C_{\alpha r}\right)}{I_x}\beta - r - \frac{I_{eq}\left(l_f C_{\alpha f} - l_r C_{\alpha r}\right)}{I_x M v_x^2} r \\
&\quad + \frac{h_{cr}\left(M g h_{cr} - K_\phi\right)}{I_x v_x}\phi - \frac{h_{cr} C_\phi}{I_x v_x}\dot\phi + \frac{I_{eq} C_{\alpha f}}{I_x M v_x}\delta \\
\dot r &= -\frac{\left(l_f C_{\alpha f} + l_r C_{\alpha r}\right)}{I_z}\beta - \frac{\left(l_f C_{\alpha f}^2 + l_r C_{\alpha r}^2\right)}{I_z v_x} r \\
&\quad + \frac{l_f C_{\alpha f}}{I_z}\delta \\
\ddot\phi &= -\frac{\left(C_{\alpha f}+C_{\alpha r}\right) h_{cr}}{I_x}\beta - \frac{\left(l_f C_{\alpha f} - l_r C_{\alpha r}\right)}{I_x v_x} r \\
&\quad + \frac{\left(M g h_{cr} - K_\phi\right)}{I_x}\phi - \frac{C_\phi}{I_x}\dot\phi + \frac{C_{\alpha f} h_{cr}}{I_x}\delta + \frac{1}{I_x} M_\phi
\end{aligned} \tag{1}$$

where δ is the wheel steering angle, and M_ϕ is the anti-roll moment which is provided by independent actuators from an active suspension system. The longitudinal velocity is denoted by v_x. The roll inertia at the contact point between the tires and the ground is given by

$$I_{eq} = I_x + M h_{cr}^2. \tag{2}$$

The vehicle position on the road is represented by the lateral position error y_L at a lookahead distance l_s and the heading error ψ_L, whose dynamics are defined as [35]

$$\begin{aligned}
\dot y_L &= v_x \beta + l_s r + v_x \psi_L \\
\dot\psi_L &= r - v_x \rho_r
\end{aligned} \tag{3}$$

where ρ_r is the road curvature. To achieve a high-performance path tracking control over a large range of look-ahead distance and vehicle speed, we consider a time-varying look-ahead distance profile of the form [36]

$$l_s(v_x) = a v_x + b \tag{4}$$

where the parameters $a = 0.36\ s$ and $b = 5\ m$ are chosen following an experimental rule.

From the vehicle model (1) and the path tracking dynamics (3), we can obtain the following state-space representation of the road-vehicle model:

$$\dot{\boldsymbol{x}} = A(v_x)\boldsymbol{x} + B(v_x)\boldsymbol{u} + D(v_x)\boldsymbol{w} \tag{5}$$

where $\boldsymbol{x} = \begin{bmatrix}\beta & r & \phi & \dot\phi & \psi_L & y_L\end{bmatrix}^\top \in \mathbb{R}^{n_x}$ is the vehicle state, $\boldsymbol{u} = \begin{bmatrix}\delta & M_\phi\end{bmatrix}^\top \in \mathbb{R}^{n_u}$ is the control input, and $\boldsymbol{w} = \rho_r \in \mathbb{R}^{n_w}$ is the disturbance, with $n_x = 6$, $n_u = 2$ and $n_w = 1$. The state-space matrices in system (5) are given by

$$A(v_x) = \begin{bmatrix}
a_{11} & a_{12} & a_{13} & a_{14} & 0 & 0 \\
a_{21} & a_{22} & 0 & 0 & 0 & 0 \\
0 & 0 & 0 & 1 & 0 & 0 \\
a_{41} & a_{42} & a_{43} & a_{44} & 0 & 0 \\
0 & 1 & 0 & 0 & 0 & 0 \\
v_x & l_s & 0 & 0 & v_x & 0
\end{bmatrix}$$

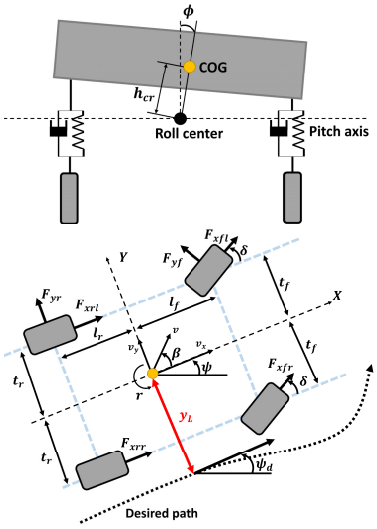

Fig. 1. Vehicle roll and lateral dynamics.

$$B(v_x)=\begin{bmatrix} \frac{I_{eq}C_{\alpha f}}{I_x m v_x} & 0 \\ \frac{l_s C_{\alpha f}}{I_z} & 0 \\ 0 & 0 \\ \frac{C_{\alpha f}h_{cr}}{I_x} & \frac{1}{I_x} \\ 0 & 0 \\ 0 & 0 \end{bmatrix}, \quad D(v_x)=\begin{bmatrix} 0 \\ 0 \\ 0 \\ 0 \\ -v_x \\ 0 \end{bmatrix}$$

$$I_{eq}=I_x+Mh_{cr}^2,\ a_{11}=-\frac{I_{eq}(C_{\alpha f}+C_{\alpha r})}{I_x M v_x}$$
$$a_{12}=-\left(1+\frac{I_{eq}(l_f C_{\alpha f}-l_r C_{\alpha r})}{I_x M v_x^2}\right)$$
$$a_{13}=\frac{h(Mgh_{cr}-K_\phi)}{I_x v_x},\ a_{14}=-\frac{h_{cr}C_\phi}{I_x v_x}$$
$$a_{21}=-\frac{l_f C_{\alpha f}-l_r C_{\alpha r}}{I_z},\ a_{22}=-\frac{l_f^2 C_{\alpha f}+l_r^2 C_{\alpha r}}{I_z v_x}$$
$$a_{41}=-\frac{(C_{\alpha f}+C_{\alpha r})h_{cr}}{I_x},\ a_{42}=-\frac{(l_f C_{\alpha f}-l_r C_{\alpha r})h_{cr}}{I_x v_x}$$
$$a_{43}=\frac{Mgh_{cr}-K_\phi}{I_x},\ a_{44}=-\frac{C_\phi}{I_x}.$$

Note that the longitudinal vehicle speed v_x can be measured with an odometer. The yaw rate r and the roll rate $\dot{\phi}$ can be obtained from an inertial measurement unit. The heading error ψ_L and the lateral deviation error y_L can be determined with a video camera or a LiDAR sensor. However, the sideslip angle β and the roll angle ϕ are difficult to obtain in practice due to expensive sensors [37], [38]. Therefore, we define the output measurement vector as $\boldsymbol{y}=\begin{bmatrix} r & \dot{\phi} & \psi_L & y_L \end{bmatrix}^\top \in \mathbb{R}^{n_y}$, with $n_y=4$, or

$$\boldsymbol{y}=C_y\boldsymbol{x}, \quad C_y=\begin{bmatrix} 0 & 1 & 0 & 0 & 0 & 0 \\ 0 & 0 & 0 & 1 & 0 & 0 \\ 0 & 0 & 0 & 0 & 1 & 0 \\ 0 & 0 & 0 & 0 & 0 & 1 \end{bmatrix}. \tag{6}$$

The controlled output $\boldsymbol{z}$ is defined to take into account the path following performance, the driving safety and comfort as

$$\boldsymbol{z}^\top\boldsymbol{z}=a_y^2+\phi^2+\dot{\phi}^2+\psi_L^2+y_L^2. \tag{7}$$

Hence, the vector $\boldsymbol{z}\in\mathbb{R}^{n_z}$, with $n_z=5$, can take the form

$$\boldsymbol{z}=C_z(v_x)\boldsymbol{x}, \quad C_z(v_x)=\begin{bmatrix} 0 & v_x & 0 & 0 & 0 & 0 \\ 0 & 0 & 1 & 0 & 0 & 0 \\ 0 & 0 & 0 & 1 & 0 & 0 \\ 0 & 0 & 0 & 0 & 1 & 0 \\ 0 & 0 & 0 & 0 & 0 & 1 \end{bmatrix}. \tag{8}$$

The vehicle dynamics (5) explicitly depends on the time-varying terms v_x, $\frac{1}{v_x}$ and $\frac{1}{v_x^2}$, which are measured and bounded as $\underline{v}_x \le v_x \le \overline{v}_x$. If v_x, $\frac{1}{v_x}$ and $\frac{1}{v_x^2}$ are *independently* considered to derive a polytopic representation for system (5), then such a representation can be complex and conservative for control design [3]. Since these speed-related terms are strongly dependent, the following change of variable can be performed to overcome this drawback [39]:

$$\frac{1}{v_x}=\frac{1}{v_0}+\frac{1}{v_1}\xi \tag{9}$$

where the new time-varying parameter ξ verifies $-1\le\xi\le 1$. Using the Taylor's approximation, we have

$$v_x\simeq v_0\left(1-\frac{v_0}{v_1}\xi\right), \quad \frac{1}{v_x^2}\simeq\frac{1}{v_0^2}\left(1+2\frac{v_0}{v_1}\xi\right) \tag{10}$$

with

$$v_0=\frac{2\underline{v}_x\overline{v}_x}{\underline{v}_x+\overline{v}_x}, \quad v_1=\frac{2\underline{v}_x\overline{v}_x}{\underline{v}_x-\overline{v}_x}.$$

Substituting (9) and (10) into (5) and (8), we can obtain the following road-vehicle model:

$$\begin{aligned} \dot{\boldsymbol{x}} &= A(\xi)\boldsymbol{x}+B(\xi)\boldsymbol{u}+D(\xi)\boldsymbol{w} \\ \boldsymbol{z} &= C_z(\xi)\boldsymbol{x} \end{aligned} \tag{11}$$

which *linearly* depends on the time-varying parameter ξ.

B. Anti-Roll Moment Distribution

The anti-roll moment is provided by the forces exerted by the actuators from the active suspension system. The force of each actuator is individually regulated and given by [40]

$$\begin{aligned} F_{fl} &= \frac{M_\phi l_r}{2t_f(l_f+l_r)}, \quad F_{fr}=-F_{fl} \\ F_{rl} &= \frac{M_\phi l_f}{2t_r(l_f+l_r)}, \quad F_{rr}=-F_{rl} \end{aligned} \tag{12}$$

where subscripts fr, fl, rr and rl refer to the front-right, front-left, rear-right and rear-left actuators, respectively.

C. Control Specifications

The control goal is to design a robust path tracking controller while taking into account the roll dynamics for autonomous vehicles with the following specifications.

- The control input must be computed only with sensors already available on series-production vehicles.
- The controller must be able to generate smooth control signals while improving the roll dynamics.
- The amount of control information transmitted over the communication network can be reduced through an event-triggering mechanism.
- The closed-loop stability and control performance is guaranteed under network-induced delays via Lyapunov-Krasovskii stability theory.

To meet these specifications, we propose in Section III a new method to design an event-triggered SOF controller such that the closed-loop LPV system (11) is stable while achieving an $\mathscr{H}_\infty$ control performance.

D. Problem Formulation

The proposed control structure is depicted in Fig. 2. The system measurements are sampled every h seconds. Then, a control signal is computed using an LPV static output feedback control scheme. The event-triggering mechanism compares the current computed control signal with the last transmitted one. If their difference exceeds a threshold, the control signal is updated and sent over the network. Then, the

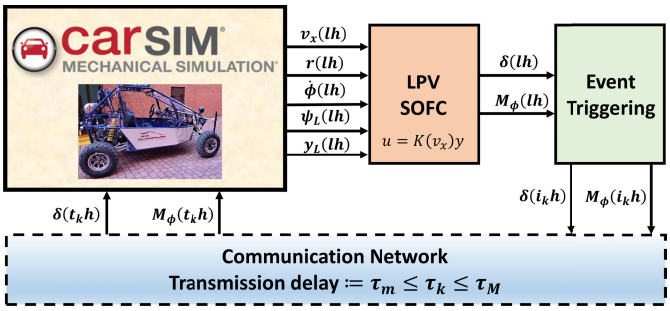

Fig. 2. General diagram for the control scheme.

control signal is transmitted to different vehicle actuators after a time communication delay.

The event-triggering mechanism consists of a register and a comparator [11]. The register keeps the information from the last released data-packet $(t_k, \boldsymbol{u}(t_k))$, for $k \in \mathbb{Z}_+$. The comparator checks if $(t, \boldsymbol{u}(t))$, with $t \in [t_k, t_{k+1})$, satisfies the event-triggering condition

$$t_{k+1} = \inf\{t > t_k : \ \mathrm{ETC}_1 \vee \mathrm{ETC}_2\} \tag{13}$$

with

$$\begin{aligned} \mathrm{ETC}_1 : \ & \boldsymbol{u}(t) \ge (1+\varepsilon)\boldsymbol{u}(t_k) \\ \mathrm{ETC}_2 : \ & \boldsymbol{u}(t) \le (1-\varepsilon)\boldsymbol{u}(t_k) \end{aligned} \tag{14}$$

where $\varepsilon > 0$ is a triggering threshold to be designed.

Remark 1: With the simple event-triggering condition (13), the basic idea is to update the control input signal only when it "significantly" changes with respect to the latest transmitted value $\boldsymbol{u}(t_k)$. The triggering parameter ε is used to specify the control update threshold.

The time delay between t and t_k is defined as

$$\eta(t) = t - t_k \tag{15}$$

with $\tau_m \le \eta(t) \le h + \tau_M$, where τ_m and τ_M are the minimum and maximum time communication delays between the network and the actuators. For control design, we consider an event-triggered SOF controller of the form

$$\boldsymbol{u}(t_k) = K(\xi_k)\boldsymbol{y}(t_k). \tag{16}$$

To deal with the asynchronous phenomenon caused by the sampling process, let us consider the following decomposition:

$$\boldsymbol{u}(t) = (1+\delta_2(t))\boldsymbol{u}(t_k), \quad t \in [t_k, t_{k+1}) \tag{17}$$

where $\delta_2(t)$ represents the error between the triggered and the current computed control signals. It follows from (13) that

$$-\varepsilon \le \delta_2(t) \le \varepsilon. \tag{18}$$

From (16) and (17), the SOF controller can be represented as

$$\boldsymbol{u}(t) = (1+\delta_2(t))K(\xi_k)\boldsymbol{y}(t_k), \ \ t \in [t_k, t_{k+1}). \tag{19}$$

Then, the vehicle closed-loop system can be formed from (11) and (19) as

$$\begin{aligned} \dot{\boldsymbol{x}}(t) &= A(\xi)\boldsymbol{x}(t) + (1+\delta_2)B(\xi)K(\xi_k)C_y\boldsymbol{x}(t_k) + D(\xi)\boldsymbol{w}(t) \\ \boldsymbol{z}(t) &= C_z(\xi)\boldsymbol{x}(t) \end{aligned} \tag{20}$$

Since the terms $\xi(t)$ and $\xi(t_k)$ are asynchronous, the following decomposition is applied for control design [41]:

$$\xi(t) = \xi(t_k) + \delta_1(t) \tag{21}$$

with $-\dot{\bar{\xi}}\bar{\eta} \le \delta_1(t) \le \dot{\bar{\xi}}\bar{\eta}$, and

$$\bar{\eta} = h + \tau_M, \quad \dot{\bar{\xi}} = \max \frac{d\xi}{dt} = \max \frac{v_1 a_x}{v_x^2}.$$

Using the sector nonlinearity approach [42, Chapter 2] while taking into account (21), the closed-loop system (22) can be expressed in a polytopic form as

$$\begin{aligned} \dot{\boldsymbol{x}}(t) &= A(\xi_k + \delta_1(t))\boldsymbol{x}(t) + D(\xi_k + \delta_1(t))\boldsymbol{w}(t) \\ &\quad + (1+\delta_2(t))B(\xi_k + \delta_1(t))K(\xi_k)C_y\boldsymbol{x}(t_k) \\ \boldsymbol{z}(t) &= C_z(\xi_k + \delta_1(t))\boldsymbol{x}(t) \end{aligned} \tag{22}$$

where

$$\begin{Bmatrix} A(\xi_k+\delta_1) \\ B(\xi_k+\delta_1) \\ D(\xi_k+\delta_1) \\ C_z(\xi_k+\delta_1) \end{Bmatrix} = \sum_{i=1}^{2}\sum_{j=1}^{2} w_{1i}(\xi_k)w_{2j}(\delta_1) \begin{Bmatrix} A_{ij} \\ B_{ij} \\ D_{ij} \\ C_{zij} \end{Bmatrix}$$

$$K(\xi_k) = \sum_{i=1}^{2} w_{1i}(\xi_k)K_i. \tag{23}$$

The state-space matrices of the linear submodels of the polytopic representation (22)–(23) are given by

$$\begin{aligned} A_{ij} &= A(\hat{\xi}_i + \hat{\delta}_{1j}), \quad B_{ij} = B(\hat{\xi}_i + \hat{\delta}_{1j}) \\ D_{ij} &= D(\hat{\xi}_i + \hat{\delta}_{1j}), \quad C_{zij} = C_z(\hat{\xi}_i + \hat{\delta}_{1j}) \end{aligned} \tag{24}$$

for $i, j \in \{1, 2\}$, with $\hat{\xi}_1 = \underline{\xi}_k$, $\hat{\xi}_2 = \bar{\xi}_k$, $\hat{\delta}_{11} = \underline{\delta}_1$, $\hat{\delta}_{12} = \bar{\delta}_1$, $\hat{\delta}_{21} = \underline{\delta}_2$ and $\hat{\delta}_{22} = \bar{\delta}_2$. The weighting functions in (23) are defined as

$$\begin{aligned} w_{11}(\xi_k) &= \frac{\bar{\xi}_k - \xi_k}{\bar{\xi}_k - \underline{\xi}_k}, \quad w_{12}(\xi_k) = 1 - w_{11}(\xi_k) \\ w_{21}(\delta_1) &= \frac{\bar{\delta}_1 - \delta_1}{\bar{\delta}_1 - \underline{\delta}_1}, \quad w_{22}(\delta_1) = 1 - w_{21}(\delta_1) \\ w_{31}(\delta_2) &= \frac{\bar{\delta}_2 - \delta_2}{\bar{\delta}_2 - \underline{\delta}_2}, \quad w_{32}(\delta_2) = 1 - w_{31}(\delta_2). \end{aligned} \tag{25}$$

The following technical lemmas are useful to design an event-triggered SOF controller (16), which verifies the control specifications stated in Section II-C.

Lemma 1 ([43]): Consider a positive definite matrix of appropriate dimension R. Then, for a continuous function ω in $[a, b]$, the following inequality holds:

$$\begin{aligned} \Xi(\omega) \ge \ & \frac{1}{b-a}\left(\int_a^b \omega(u)du\right)^\top R \left(\int_a^b \omega(u)du\right) \\ & + \frac{3}{b-a}\Omega^\top R \Omega \end{aligned} \tag{26}$$

where

$$\begin{aligned} \Xi(\omega) &= \int_a^b \omega^\top(u) R \omega(u) du \\ \Omega &= \int_a^b \omega(s)ds - \frac{2}{b-a}\int_a^b \int_a^s \omega(r)drds. \end{aligned} \tag{27}$$

Lemma 2 ([44]): For given positive integers n, m, a scalar $\alpha \in (0,1)$, a positive definite matrix $R \in \mathbb{R}^{n\times n}$, and two matrices $W_1 \in \mathbb{R}^{n\times m}$ and $W_2 \in \mathbb{R}^{n\times m}$. Define, for any $\boldsymbol{\xi} \in \mathbb{R}^m$, the function $\Theta(\alpha, R)$ as

$$\Theta(\alpha, R) = \frac{1}{\alpha}\boldsymbol{\xi}^\top W_1^\top R W_1 \boldsymbol{\xi} + \frac{1}{1-\alpha}\boldsymbol{\xi}^\top W_2^\top R W_2 \boldsymbol{\xi}. \tag{28}$$

If there exists a matrix $X \in \mathbb{R}^{n\times n}$ such that $\begin{bmatrix} R & X \\ * & R \end{bmatrix} > 0$, then the following inequality holds:

$$\min_{\alpha\in(0,1)} \Theta(\alpha, R) \geq \begin{bmatrix} W_1\boldsymbol{\xi} \\ W_2\boldsymbol{\xi} \end{bmatrix}^\top \begin{bmatrix} R & X \\ * & R \end{bmatrix} \begin{bmatrix} W_1\boldsymbol{\xi} \\ W_2\boldsymbol{\xi} \end{bmatrix}. \tag{29}$$

III. Event-Triggered Control Design

The following theorem presents Lyapunov-Krasovskii-based conditions to design an $\mathscr{H}_\infty$ event-triggered SOF controller for path tracking with roll dynamics improvements.

Theorem 1: For given scalars $h > 0$, $\tau_M \geq \tau_m > 0$ and μ, if there exist positive definite matrices $\tilde{P} \in \mathbb{R}^{n_x\times n_x}$, $\tilde{R} \in \mathbb{R}^{n_x\times n_x}$, $\tilde{U} \in \mathbb{R}^{n_x\times n_x}$, symmetric matrices $\tilde{S} \in \mathbb{R}^{n_x\times n_x}$, $\tilde{Q} \in \mathbb{R}^{n_x\times n_x}$, matrices $X \in \mathbb{R}^{n_x\times n_x}$, $Y_1 \in \mathbb{R}^{n_x\times 4n_x}$, $Y_2 \in \mathbb{R}^{n_x\times 4n_x}$, $K_i \in \mathbb{R}^{n_u\times n_y}$, for $i \in \{1,2\}$, and a positive scalar γ such that LMI conditions (30), (31) and (32) are feasible. Then, the closed-loop system (22) is stable with an $\mathscr{H}_\infty$ performance index less than or equal to γ.

$$\begin{bmatrix} \tilde{Q} & \tilde{S}^\top - \tilde{Q} \\ * & \tilde{Q} - \tilde{S} - \tilde{S}^\top \end{bmatrix} \geq 0, \quad \tilde{U} \geq 0 \tag{30}$$

$$\Theta_{1ijl}(h_k) < 0 \tag{31}$$

$$\Theta_{2ijl}(h_k) < 0 \tag{32}$$

for $i, j, l \in \{1,2\}$ and $h_k \in \{\tau_m, \tau_M + h\}$, where

$$\begin{aligned}
\Theta_{1ijl}(h_k) &= \tilde{\Pi}_{1ijl} + h_k(\tilde{\Pi}_2 + \tilde{\Pi}_3) \\
\Theta_{2ijl}(h_k) &= \begin{bmatrix} \tilde{\Pi}_{1ijl} - h_k\tilde{\Pi}_3 & h_k W_3^\top \tilde{Y}_1^\top & 3\,h_k W_3^\top \tilde{Y}_2^\top \\ * & -h_k\tilde{R} & 0 \\ * & * & -3h_k R \end{bmatrix} \\
\tilde{\Pi}_{1ijl} &= \tilde{\Pi}_1^0 + \tilde{\Pi}_{1ij}^1 + \tilde{\Pi}_{1ijl}^2 + \tilde{\Pi}_{1ij}^3 - \gamma^2 M_5^\top M_5 \\
&\quad - \mathrm{He}\left\{W_3^\top \tilde{Y}_1^\top W_1 + 3W_3^\top \tilde{Y}_2^\top W_2\right\} \\
&\quad + \mathrm{He}\left\{M_1^\top X^\top C_z^\top (\xi_i + \delta_{1j}) M_6\right\} - M_6^\top M_6 \\
\tilde{\Pi}_1^0 &= \mathrm{He}\left\{M_1^\top \tilde{P} M_4 - W_1^\top \tilde{Q} M_2 \right. \\
&\quad \left. -(M_1^\top + \mu M_2^\top + \mu M_4^\top) X M_4\right\} - W_1^\top \tilde{S} W_1 \\
\tilde{\Pi}_{1ij}^1 &= \mathrm{He}\left\{(M_1^\top + \mu M_2^\top + \mu M_4^\top) A(\xi_i + \delta_{1j}) X M_1\right\} \\
\tilde{\Pi}_{1ijl}^2 &= \mathrm{He}\left\{(M_1^\top + \mu M_2^\top + \mu M_4^\top) \right. \\
&\quad \left. \times B(\xi_i + \delta_{1j})(1 + \delta_{2l}) K_i C_y X M_2\right\} \\
\tilde{\Pi}_{1ij}^3 &= \mathrm{He}\left\{(M_1^\top + \mu M_2^\top + \mu M_4^\top) D(\xi_i + \delta_{1j}) M_5\right\} \\
\tilde{\Pi}_2 &= M_4^\top \tilde{R} M_4 + \mathrm{He}\left\{M_4^\top \tilde{S} W_1 + M_4^\top \tilde{Q} M_2\right\} \\
\tilde{\Pi}_3 &= M_2^\top \tilde{U} M_2 \\
M_1 &= \begin{bmatrix} I & 0 & 0 & 0 & 0 & 0 \end{bmatrix} \\
M_2 &= \begin{bmatrix} 0 & I & 0 & 0 & 0 & 0 \end{bmatrix} \\
M_3 &= \begin{bmatrix} 0 & 0 & I & 0 & 0 & 0 \end{bmatrix} \\
M_4 &= \begin{bmatrix} 0 & 0 & 0 & I & 0 & 0 \end{bmatrix} \\
M_5 &= \begin{bmatrix} 0 & 0 & 0 & 0 & I & 0 \end{bmatrix} \\
M_6 &= \begin{bmatrix} 0 & 0 & 0 & 0 & 0 & I \end{bmatrix} \\
W_1 &= M_1 - M_2 \\
W_2 &= M_1 + M_2 - 2M_3 \\
W_3 &= M_1 + M_2 + M_3 + M_4.
\end{aligned}$$

Proof: For the closed-loop stability analysis, we consider the following Lyapunov-Krasovskii functional:

$$V(t) = V_1(t) + V_2(t) + V_3(t) + V_4(t) \tag{33}$$

with

$$\begin{aligned}
V_1(t) &= \boldsymbol{x}^\top(t) P \boldsymbol{x}(t) \\
V_2(t) &= (h_k - \eta(t))(\boldsymbol{x}(t) - \boldsymbol{x}(t_k))^\top S(\boldsymbol{x}(t) - \boldsymbol{x}(t_k)) \\
&\quad + \mathrm{He}\left\{(h - \eta(t))(\boldsymbol{x}(t) - \boldsymbol{x}(t_k))^\top Q \boldsymbol{x}(t_k)\right\} \\
V_3(t) &= (h_k - \eta(t)) \int_{t_k}^{t} \dot{\boldsymbol{x}}^\top(s) R \dot{\boldsymbol{x}}(s) ds \\
V_4(t) &= (h_k - \eta(t))(t - t_k)\eta(t) \boldsymbol{x}^\top(t_k) U \boldsymbol{x}(t_k)
\end{aligned} \tag{34}$$

where h_k denotes the time interval between two successive data received by the actuators, the matrices $P \in \mathbb{R}^{n_x\times n_x}$ and $R \in \mathbb{R}^{n_x\times n_x}$ are symmetric positive definite, and S, Q and U are symmetric. We consider the changes of variables

$$\begin{aligned}
&\tilde{P} = X^\top P X, \quad \tilde{R} = X^\top R X, \ \tilde{U} = X^\top U X \\
&\tilde{S} = X^\top S X, \quad \tilde{Q} = X^\top Q X.
\end{aligned} \tag{35}$$

With the changes of variables (35) and following similar arguments as in [45, Lemma 2], we can prove that condition (30) ensures the positiveness of the Lyapunov-Krasovskii functional (34). The time derivative of $V(t)$ in (34) is given by

$$\dot{V}(t) = \dot{V}_1(t) + \dot{V}_2(t) + \dot{V}_3(t) + \dot{V}_4(t) \tag{36}$$

where

$$\begin{aligned}
\dot{V}_1(t) &= \mathrm{He}\left\{\boldsymbol{x}^\top(t) P \dot{\boldsymbol{x}}(t)\right\} \\
\dot{V}_2(t) &= -(\boldsymbol{x}(t) - \boldsymbol{x}(t_k))^\top S(\boldsymbol{x}(t) - \boldsymbol{x}(t_k)) \\
&\quad - \mathrm{He}\left\{(\boldsymbol{x}(t) - \boldsymbol{x}(t_k))^\top Q \boldsymbol{x}(t_k)\right\} \\
&\quad + (t_{k+1} - t)\mathrm{He}\left\{\dot{\boldsymbol{x}}^\top(t) S(\boldsymbol{x}(t) - \boldsymbol{x}(t_k))\right\} \\
&\quad + (t_{k+1} - t)\mathrm{He}\left\{\dot{\boldsymbol{x}}^\top(t) Q \boldsymbol{x}(t_k)\right\} \\
\dot{V}_3(t) &= -\int_{t_k}^{t} \dot{\boldsymbol{x}}^\top(s) R \dot{\boldsymbol{x}}(s) ds + (t_{k+1} - t)\dot{\boldsymbol{x}}^\top(t) R \dot{\boldsymbol{x}}(t) \\
\dot{V}_4(t) &= -(t - t_k)\boldsymbol{x}^\top(t_k) U \boldsymbol{x}(t_k) + (t_{k+1} - t)\boldsymbol{x}^\top(t_k) U \boldsymbol{x}(t_k).
\end{aligned}$$

Let us define the augmented vector

$$\boldsymbol{\zeta}(t) = \left[\boldsymbol{x}^\top(t) \ \boldsymbol{x}^\top(t_k) \ \boldsymbol{v}_k^\top(t) \ \dot{\boldsymbol{x}}^\top(t) \ \boldsymbol{w}^\top(t)\right]^\top \tag{37}$$

with

$$\boldsymbol{v}_k(t) = \frac{1}{\eta}\int_{t_k}^{t} \boldsymbol{x}(s) ds. \tag{38}$$

Applying Lemma 1, the first term of $\dot{V}_3(\eta, x)$ in (36) can be bounded as

$$-\int_{t_k}^{t} \dot{\boldsymbol{x}}^\top(s) R \dot{\boldsymbol{x}}(s) ds \leq -\frac{1}{\eta} \boldsymbol{\zeta}^\top (W_1^\top R W_1 + 3 W_2^\top R W_2) \boldsymbol{\zeta}. \tag{39}$$

Moreover, it follows from Lemma 2 that there exist matrices Y_1 and Y_2 such that

$$\begin{aligned} -\frac{1}{\eta} W_1^\top R W_1 &\leq -\mathrm{He}\left\{Y_1^\top W_1\right\} + \eta Y_1^\top R^{-1} Y_1 \\ -\frac{1}{\eta} W_2^\top R W_2 &\leq -\mathrm{He}\left\{Y_2^\top W_2\right\} + \eta Y_2^\top R^{-1} Y_2 \end{aligned} \tag{40}$$

For any vector $\boldsymbol{\zeta}(t)$, and any matrices of appropriate dimensions M_1, M_2, M_4 and X, the following algebraic relation can be directly deduced from (22):

$$\begin{aligned} &\boldsymbol{\zeta}^\top(t)(M_1^\top + \mu M_2^\top + \mu M_4^\top) X^{-\top} \\ &\quad \times \left\{A(\xi_k + \delta_1)\boldsymbol{x}(t) + (1+\delta_2) B(\xi_k + \delta_1) K(\xi_k) C_y \boldsymbol{x}(t_k) \right. \\ &\quad \left. + D(\xi_k + \delta_1)\boldsymbol{w}(t) - \dot{\boldsymbol{x}}(t)\right\} = 0. \end{aligned} \tag{41}$$

By symmetry and by the definition of $\boldsymbol{\zeta}(t)$ in (37), it follows from (41) that

$$\begin{aligned} &\mathrm{He}\left\{\boldsymbol{\zeta}^\top(t)\mathbf{M}X^{-\top} A(\xi_k + \delta_1) M_1 \boldsymbol{\zeta}(t) \right. \\ &\quad + \boldsymbol{\zeta}^\top(t)\mathbf{M}X^{-\top}(1+\delta_2) B(\xi_k + \delta_1) K(\xi_k) C_y M_2 \boldsymbol{\zeta}(t) \\ &\quad + \boldsymbol{\zeta}^\top(t)\mathbf{M}X^{-\top} D(\xi_k + \delta_1) M_5 \boldsymbol{\zeta}(t) \\ &\quad \left. - \boldsymbol{\zeta}^\top(t)\mathbf{M}X^{-\top} M_4 \boldsymbol{\zeta}(t)\right\} = 0 \end{aligned} \tag{42}$$

with $\mathbf{M} = M_1^\top + \mu M_2^\top + \mu M_4^\top$. For control design, we consider the $\mathscr{H}_\infty$ performance as [46]

$$\dot{V}(t) + \boldsymbol{z}^\top(t)\boldsymbol{z}(t) - \gamma^2 \boldsymbol{w}^\top(t)\boldsymbol{w}(t) < 0 \tag{43}$$

where the positive scalar γ is to be minimized for disturbance attenuation. From (39), (40), (42) and (43), the upper bound of the time derivative of Lyapunov-Krasovskii functional defined in (36) can be derived as

$$\dot{V}(t) \leq \boldsymbol{\zeta}(t)^\top \Pi(\eta, h_k, \boldsymbol{\rho}) \boldsymbol{\zeta}(t) \tag{44}$$

where $\boldsymbol{\rho}(t) = \left[\xi_k \ \delta_1(t) \ \delta_2(t)\right]^\top$, and

$$\Pi(\eta, h_k, \boldsymbol{\rho}) = \Pi_1(\boldsymbol{\rho}) + (h_k - \eta)\Pi_2 + (h_k - 2\eta)\Pi_3 + \eta \Pi_4 \tag{45}$$

with

$$\begin{aligned} \Pi_1(\boldsymbol{\rho}) &= \Pi_0^1 + \Pi_1^1(\boldsymbol{\rho}) + \Pi_1^2(\boldsymbol{\rho}) + \Pi_1^3(\boldsymbol{\rho}) - \gamma^2 M_5^\top M_5 \\ &\quad - \mathrm{He}\left\{W_3^\top Y_1^\top W_1 + 3 W_3^\top Y_2^\top W_2\right\} \\ &\quad + \mathrm{He}\left\{M_1^\top C_z^\top (\xi_k + \delta_1) M_6\right\} - M_6^\top M_6 \\ \Pi_0^1 &= \mathrm{He}\left\{M_1^\top P M_4 - W_1^\top Q M_2 - \mathbf{M}X^{-\top} M_4\right\} - W_1^\top S W_1 \\ \Pi_1^1(\boldsymbol{\rho}) &= \mathrm{He}\left\{\mathbf{M}X^{-\top} A(\xi_k + \delta_1) M_1\right\} \\ \Pi_1^2(\boldsymbol{\rho}) &= \mathrm{He}\left\{\mathbf{M}X^{-\top} B(\xi_k + \delta_1)(1+\delta_2) K(\xi_k) C_y M_2\right\} \\ \Pi_1^3(\boldsymbol{\rho}) &= \mathrm{He}\left\{\mathbf{M}X^{-\top} D(\xi_k + \delta_1) M_5\right\} \\ \Pi_2 &= M_4^\top R M_4 + \mathrm{He}\left\{M_4^\top S W_1 + M_4^\top Q M_2\right\} \\ \Pi_3 &= M_2^\top U M_2 \\ \Pi_4 &= W_3^\top Y_1^\top R^{-1} Y_1 W_3 + W_3^\top Y_2^\top R^{-1} Y_2 W_3. \end{aligned}$$

Since the expression of $\Pi(\eta, h_k, \boldsymbol{\rho})$ in (45) is affine with respect to $\eta(t)$, then $\Pi(\eta, h_k, \boldsymbol{\rho}) < 0$ if $\Pi(0, h_k, \boldsymbol{\rho}) < 0$ and $\Pi(h_k, h_k, \boldsymbol{\rho}) < 0$, or respectively

$$\Pi_1(\boldsymbol{\rho}) + h_k \Pi_2 + h_k \Pi_3 < 0 \tag{46}$$

$$\begin{bmatrix} \Pi_1(\boldsymbol{\rho}) - h_k \Pi_3 & h_k W_3^\top Y_1^\top & 3\, h_k W_3^\top Y_2^\top \\ * & -h_k R & 0 \\ * & * & -3\, h_k R \end{bmatrix} < 0. \tag{47}$$

Applying the congruence transformations to conditions (46) and (47) with the following respective matrices:

$$\begin{aligned} &\mathrm{diag}\left\{X^\top, X^\top, X^\top, X^\top, I, I\right\} \\ &\mathrm{diag}\left\{X^\top, X^\top, X^\top, X^\top, I, I, X^\top, X^\top\right\} \end{aligned} \tag{48}$$

we can obtain

$$\Theta_1(h_k, \boldsymbol{\rho}) < 0 \tag{49}$$

$$\Theta_2(h_k, \boldsymbol{\rho}) < 0 \tag{50}$$

with

$$\begin{aligned} \Theta_1(h_k, \boldsymbol{\rho}) &= \tilde{\Pi}_1(\boldsymbol{\rho}) + h_k \tilde{\Pi}_2 + h_k \tilde{\Pi}_3 \\ \Theta_2(h_k, \boldsymbol{\rho}) &= \begin{bmatrix} \tilde{\Pi}_1(\boldsymbol{\rho}) - h_k \tilde{\Pi}_3 & h_k W_3^\top \tilde{Y}_1^\top & 3\, h_k W_3^\top \tilde{Y}_2^\top \\ * & -h_k \tilde{R} & 0 \\ * & * & -3\, h_k \tilde{R} \end{bmatrix}. \end{aligned}$$

Considering the polytopic representation (23), the expressions of $\Theta_1(h_k, \boldsymbol{\rho})$ and $\Theta_2(h_k, \boldsymbol{\rho})$ can be rewritten as

$$\begin{aligned} \Theta_1(h_k, \boldsymbol{\rho}) &= \sum_{i=1}^{2}\sum_{j=1}^{2}\sum_{l=1}^{2} w_{1i}(\xi_k) w_{2j}(\delta_1) w_{3l}(\delta_2) \Theta_{1ijl}(h_k) \\ \Theta_2(h_k, \boldsymbol{\rho}) &= \sum_{i=1}^{2}\sum_{j=1}^{2}\sum_{l=1}^{2} w_{1i}(\xi_k) w_{2j}(\delta_1) w_{3l}(\delta_2) \Theta_{2ijl}(h_k). \end{aligned} \tag{51}$$

With the polytopic representation (51), it is clear that conditions (31) and (32) ensure (49) and (50), repectively. This completes the proof. ■

Since the decision variables X and K_i, for $i \in \{1, 2\}$, are coupled in conditions (31) and (32), the control design conditions in Theorem 1 are expressed in terms of bilinear matrix inequalities. We propose in Algorithm 1 an LMI-based iterative procedure to find an *offline* SOF control solution. A similar design procedure with discussions on the convergence of such iterative algorithms can be found in [47].

Remark 2: The LMI-based control design procedure in Algorithm 1 can be implemented with any suitable semidefinite programming software [48]. Here, YALMIP parser and MOSEK solver are used to find a feasible SOF control solution.

Algorithm 1 Iterative Procedure for SOF Control Design

Input: Vehicle parameters in Table I, delay characteristics τ_m and τ_M, sampling time h, user-defined tolerance ϵ, maximum number of iterations $k_{\max}$.

Output: Event-triggered SOF controller (16).

Initialization:

- Set $C_y = I$ and $\tilde{K}_i^{sf} = K_i^{sf} X$, $i \in \{1, 2\}$
- Solve LMI conditions (30)–(32)
- Get K_i^{sf}, $i \in \{1, 2\}$, with the optimal value $\gamma_{\min} = \gamma^{(0)}$
- Set C_y as in (6), obtain $K_i^{(1)} = C_y K_i^{sf}$, $i \in \{1, 2\}$

for $k = 1 : k_{\max}$ **do**

1: Given $K_i^{(k)}$, solve LMIs (30)–(32) to get $X^{(k)}$
2: Given $X^{(k)}$, solve LMIs (30)–(32) to get $K_i^{(k+1)}$ and $\gamma^{(k)}$
3: **if** $|\gamma^{(k)} - \gamma^{(k-1)}|/\gamma^{(k)} < \epsilon$ **then**
4: Stop
5: **end if**

end for

IV. Illustrative Results and Discussions

This section illustrates the effectiveness of the proposed event-triggered SOF path tracking control method. To this end, all the test scenarios are performed with an experimental-validated Goka 650 buggy in the CarSim platform under various driving maneuvers. The communication network and event-triggering parameters used in this paper are summarized in Table II. For all the tests, the upper bound of network-induced delays in the vehicle control system is around 1.7 h as discussed in [49] and [50]. Moreover, a minimum network delay of 2 ms is assumed as in [51]. The vehicle speed is bounded as $\underline{v}_x = 5\ m/s$ and $\overline{v}_x = 30\ m/s$. The maximum vehicle longitudinal acceleration is assumed as $\overline{a}_x = 4\ m/s^2$. Therefore, the bounds of the time-varying parameters of system (20), which are used to determine the polytopic representation (22), are given by

$$|\xi_k| \leq 1, \quad |\delta_1| \leq 0.1152, \quad |\delta_2| \leq 0.05.$$

Applying the LMI-based design procedure in Algorithm 1 with $\mu = 0.5$, $k_{\max} = 20$, the SOF control gains are obtained as

$$K_1 = \begin{bmatrix} -0.3730 & -0.0926 & -0.3018 & -0.1995 \\ -656.33 & -1094.03 & 3825.48 & -322.60 \end{bmatrix}$$
$$K_2 = \begin{bmatrix} -0.1337 & -0.0760 & -0.2775 & -0.16486 \\ -1592.28 & -2633.88 & 3014.78 & -2363.62 \end{bmatrix}.$$

The normalized load transfer (NLT) provides an accurate index to evaluate the roll stability control [52]. Hence, for the ride safety evaluation, we compute the NLT indices for both axles as

$$NLT_f = \frac{\Delta F_{zf}}{F_{zf}}, \quad NLT_r = \frac{\Delta F_{zr}}{F_{zr}} \tag{52}$$

where F_{zf} and F_{zr} are the total load on the front axle and the rear axle, defined as

$$F_{zf} = \frac{l_r}{l_f + l_r} Mg, \quad F_{zr} = \frac{l_f}{l_f + l_r} Mg. \tag{53}$$

TABLE II
Network-Delay and Event-Triggering Parameters

Parameter	Value
h	10 ms
τ_m	2 ms
τ_M	17 ms
ε	5%

The lateral load transfer values ΔF_{zf} and ΔF_{zr} for the front axle and the rear axle are defined as

$$\Delta F_{zf} = \frac{K_\phi \phi}{t_f}, \quad \Delta F_{zr} = \frac{K_\phi \phi}{t_r}. \tag{54}$$

Note that the rollover does not occur if $-1 < NLT < 1$.

For performance comparison purposes, we consider the following path tracking controllers.

- PI control. This inbuilt PI controller in CarSim is only concerned with the steering control, *i.e.*, $M_\phi = 0$.
- LQR control. The event-triggered LQR control, whose design is adapted from [16] to take into account the in-vehicle communication delay and the asynchronous phenomenon caused by the sampling process.
- MPC control. The event-triggered MPC controller, whose design is adapted from the offline LMI-based formulation in [53] to take into account the in-vehicle communication delay and the asynchronous phenomenon caused by the sampling process.
- SOF control. The event-triggered robust SOF controller is designed with the design procedure in Algorithm 1.
- State feedback (SF) control. The event-triggered robust SF controller is designed from the conditions in Theorem 1, assuming that $C_y = I$, *i.e.*, all the vehicle states are measurable. This SF controller is used to show that the proposed SOF controller can achieve a similar control performance even with less vehicle sensors.

A. Scenario 1: Double Lane Change Maneuver

For the considered double lane change (DLC) maneuver, the vehicle speed is set as $v_x = 100\ km/h$. The vehicle response during this maneuver is depicted in Figs. 3–5. Moreover, the performance indicators, including the maximal tracking errors, the root means squared (RMS) tracking errors, the NLT index, and the network transmission rate, are summarized in Table III. With a maximum lateral error of 0.75 m, the proposed SOF controller provides a better path tracking performance than the PI, LQR and MPC controllers, yielding 1.32 m, 0.89 m and 0.86 m, respectively. In terms of driving safety, the PI, LQR and MPC controllers lead the worst results with the NLT values of 0.55, 0.41 and 0.44, respectively. The ride comfort is also improved with the proposed controller since the power spectral densities (PSD) of the lateral acceleration are lower than those of the PI, LQR and MPC controllers. The proposed event-triggering mechanism retrieves a transmission rate of 57.12%. In particular, the path tracking control results obtained with the SOF and SF controllers are very similar. This indicates that with the proposed control method, the overall control performance is not significantly affected even if some

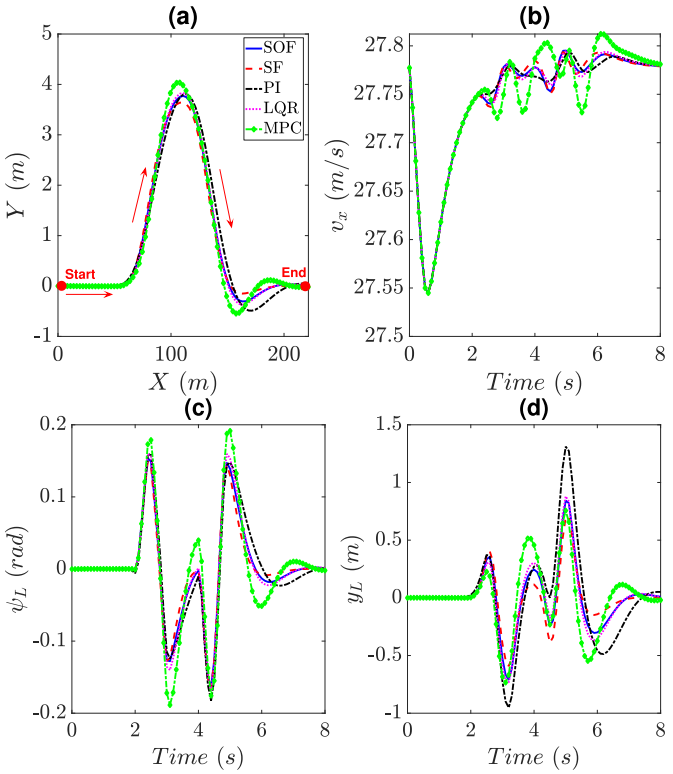

Fig. 3. Path tracking performance obtained with a DLC maneuver at a high vehicle speed. (a) Path tracking, (b) Vehicle longitudinal speed, (c) Heading error, (d) Lateral error.

TABLE III

PERFORMANCE INDICATORS WITH A DLC MANEUVER

Indicator	SOF	SF	PI	LQR	MPC
RMS ψ_L (rad)	0.063	0.060	0.069	0.067	0.079
$\psi_{L\,\max}$ (rad)	0.165	0.167	0.183	0.170	0.194
RMS y_L (m)	0.266	0.220	0.412	0.290	0.291
$y_{L\,\max}$ (m)	0.757	0.724	1.326	0.890	0.861
$NLT_{\max}$ $(-)$	0.314	0.184	0.557	0.417	0.440
Transmission rate	57.12%	59.37%	100%	55.87%	70.50%

costly sensors are not required for control implementation. Remark also that the PI controller can achieve small tracking errors. However, this controller does not consider the roll behavior, the vehicle dynamics can be compromised over time.

B. Scenario 2: Driving With a Race Course Track

For this scenario, the longitudinal speed varies according to the path curvature, which is controlled by the inbuilt PI speed controller in CarSim. This test allows analyzing the performance of the considered controllers with a time-varying vehicle speed profile. The corresponding vehicle response is depicted through Figs. 6–8, and the performance indicators are summarized in Table IV. Concerning the path tracking errors, the best results are achieved by the proposed controller, with a maximum lateral error of 0.40 m, while the PI, LQR and MPC controllers return 0.76 m, 0.43 m and 0.47 m, respectively. With the proposed controller, the maximum NLT is 0.30, which is lower than the ones obtained with the PI, LQR and MPC controllers, *i.e.*, 0.58, 0.41 and 0.42, respectively. This means that the proposed SOF controller can enhance the ride

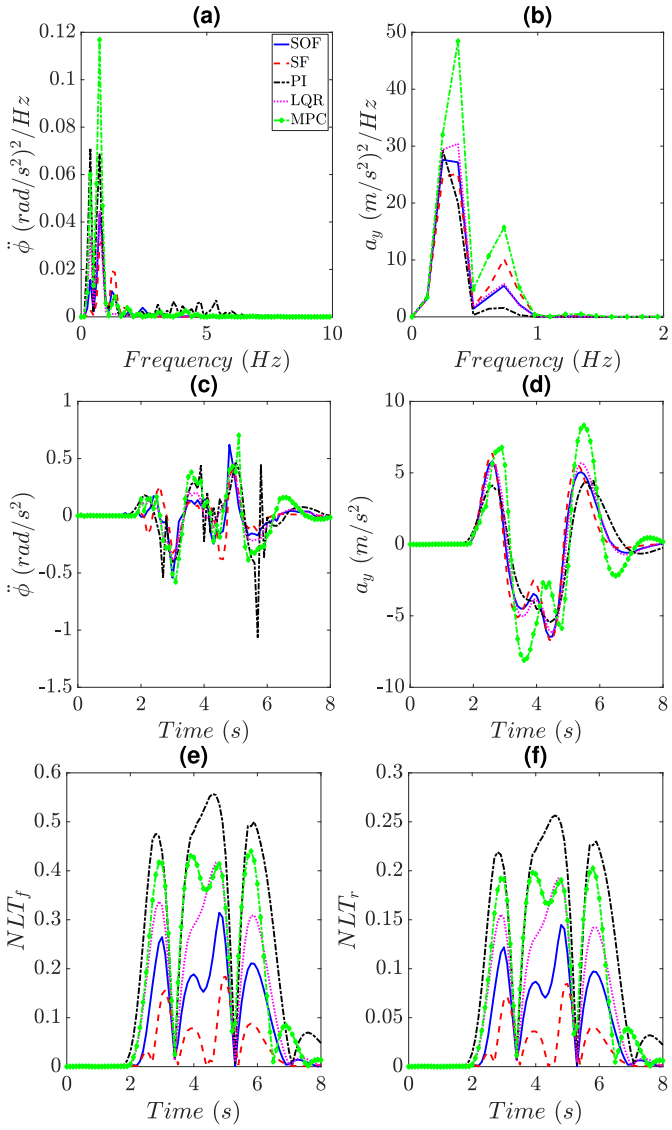

Fig. 4. Vehicle behavior obtained with a DLC maneuver at a high vehicle speed. (a) Roll acceleration PSD, (b) Lateral acceleration PSD, (c) Roll acceleration, (d) Lateral acceleration, (e) NLT of the front axle, (f) NLT of the rear axle.

TABLE IV

PERFORMANCE INDICATORS WITH A RACE TRACK COURSE

Indicator	SOF	SF	PI	LQR	MPC
RMS ψ_L (rad)	0.158	0.158	0.158	0.158	0.156
$\psi_{L\,\max}$ (rad)	0.397	0.386	0.398	0.402	0.382
RMS y_L (m)	0.086	0.138	0.153	0.107	0.081
$y_{L\,\max}$ (m)	0.402	0.299	0.760	0.439	0.476
$NLT_{\max}$ $(-)$	0.306	0.439	0.587	0.414	0.428
Transmission rate	27.04%	32.62%	100%	33.87%	36.04%

safety. In terms of ride comfort, the PI controller provides the worst result about the PSD of the roll acceleration, which is similar for other controllers. The network communication is also enhanced with the proposed event-triggering mechanism with a transmission rate of 27.04%.

C. Scenario 3: J-Turn Maneuver

To highlight the importance of the coupled lateral-roll dynamics, the vehicle behavior is now evaluated under a J-turn

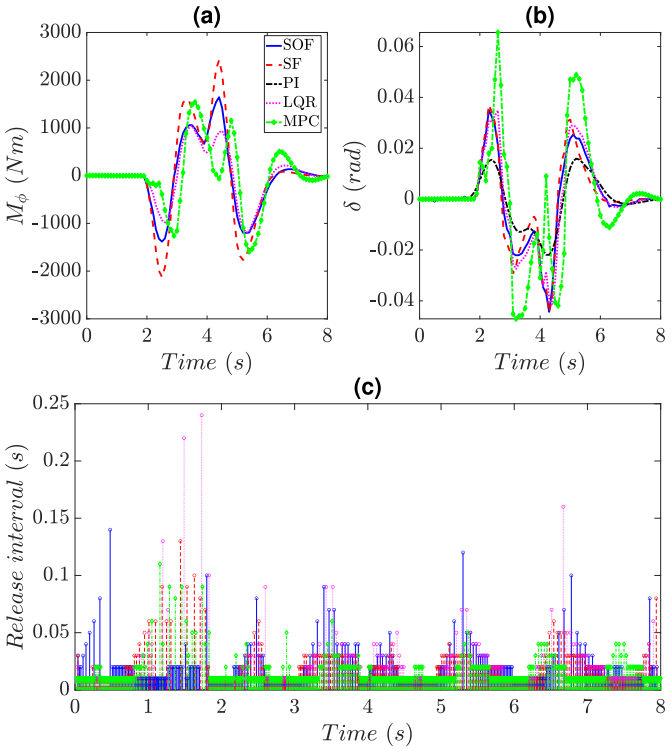

Fig. 5. Control performance obtained with a DLC maneuver at a high vehicle speed. (a) Anti-roll moment, (b) Steering angle, (c) Event-triggering instants.

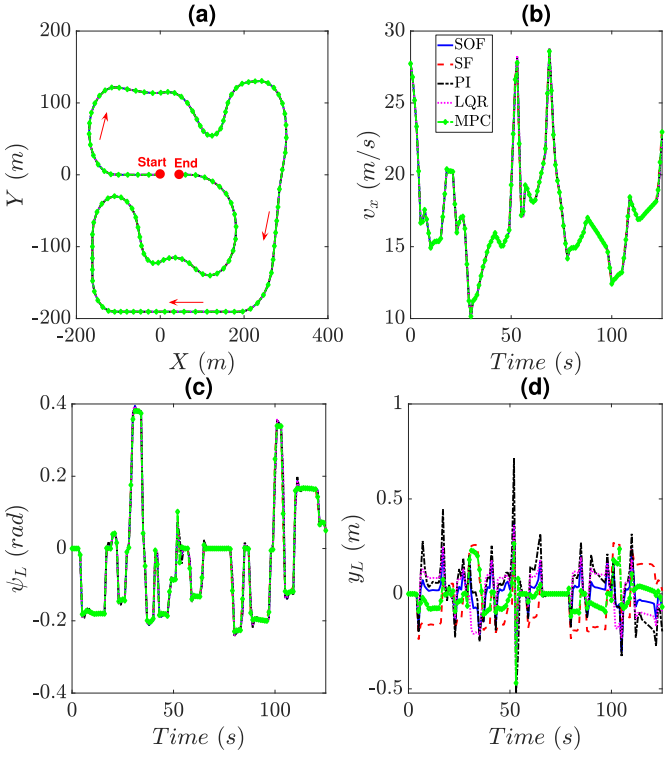

Fig. 6. Path tracking performance obtained with a race course track and a time-varying speed. (a) Path tracking, (b) Vehicle longitudinal speed, (c) Heading error, (d) Lateral error.

maneuver with a radius of 152.4 m, an increasing longitudinal speed profile from 0 to 30 m/s, and a constant acceleration of $a_x = 4\ m/s^2$. The results obtained with test scenario

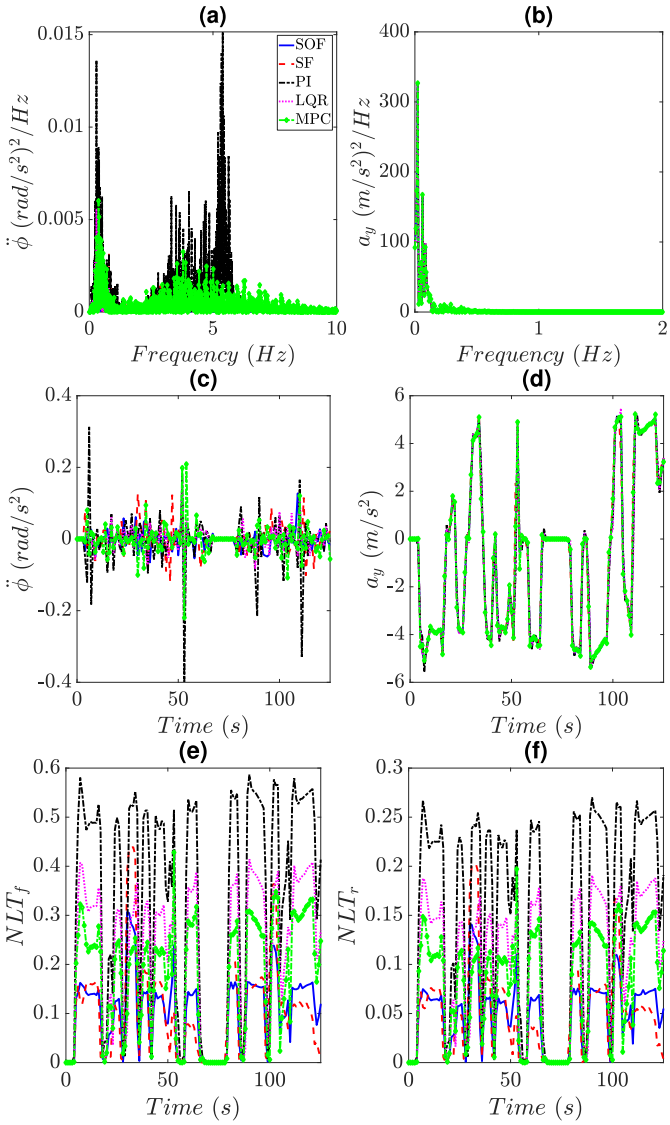

Fig. 7. Vehicle behavior obtained with a race track and a time-varying speed. (a) Roll acceleration PSD, (b) Lateral acceleration PSD, (c) Roll acceleration, (d) Lateral acceleration, (e) NLT of the front axle, (f) NLT of the rear axle.

TABLE V

PERFORMANCE INDICATORS WITH A J-TURN MANEUVER

Indicator	SOF	SF	PI	LQR	MPC
RMS $\psi_L\ (rad)$	0.008	0.008	0.008	0.008	0.008
$\psi_{L\max}\ (rad)$	0.018	0.019	0.015	0.018	0.021
RMS $y_L\ (m)$	0.070	0.112	0.214	0.085	0.189
$y_{L\max}\ (m)$	0.181	0.162	0.745	0.124	0.248
$NLT_{\max}\ (-)$	0.162	0.149	0.500	0.364	0.329
Transmission rate	23.07%	24.80%	100%	24.53%	23.73%

are presented in Figs. 9–11, and the performance indicators are summarized in Table V. Due to the extreme severity of this maneuver with very high speed and lateral acceleration, the most important performance indicators are the maximum lateral error and the maximum NLT. The maximum lateral error is lower with the proposed SOF controller (0.18 m) than the ones obtained with the PI and MPC controllers (0.74 m and 0.24 m, respectively). Concerning the roll stability, the PI, LQR and MPC controllers respectively yield a maximum NLT of 0.50, 0.36 and 0.32, which is further enhanced

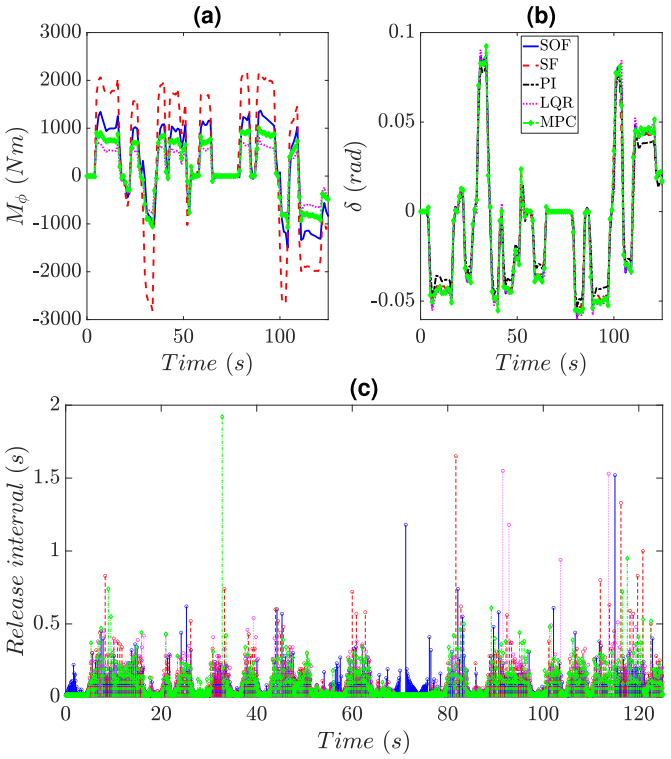

Fig. 8. Control performance obtained with a race course track and a time–varying speed. (a) Anti-roll moment, (b) Steering angle, (c) Event-triggering instants.

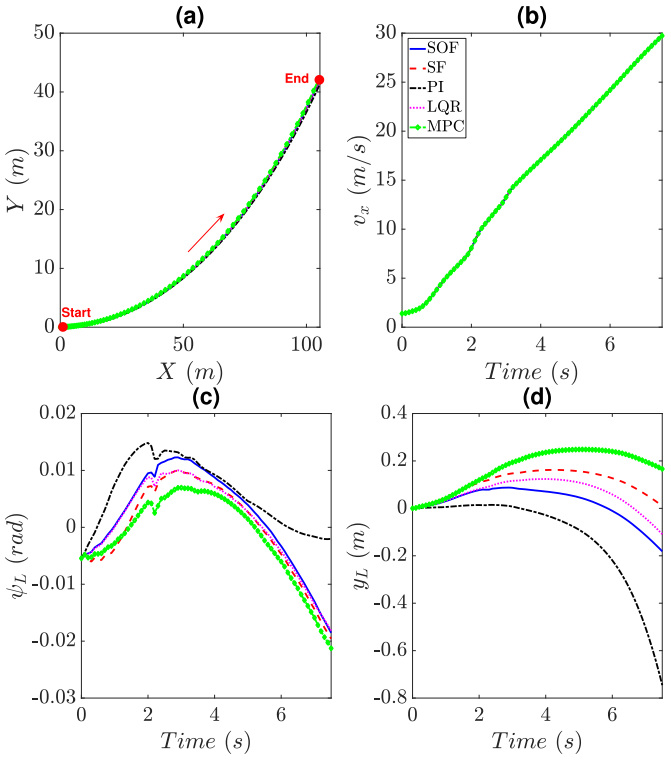

Fig. 9. Path tracking performance obtained with a J-turn maneuver and an increasing vehicle speed profile. (a) Path tracking performance, (b) Vehicle longitudinal speed, (c) Heading error, (d) Lateral error.

by the proposed controller with a maximum NLT of 0.16. Moreover, the proposed event-triggering mechanism retrieves a transmission rate of 23.07% for this test scenario. Although a

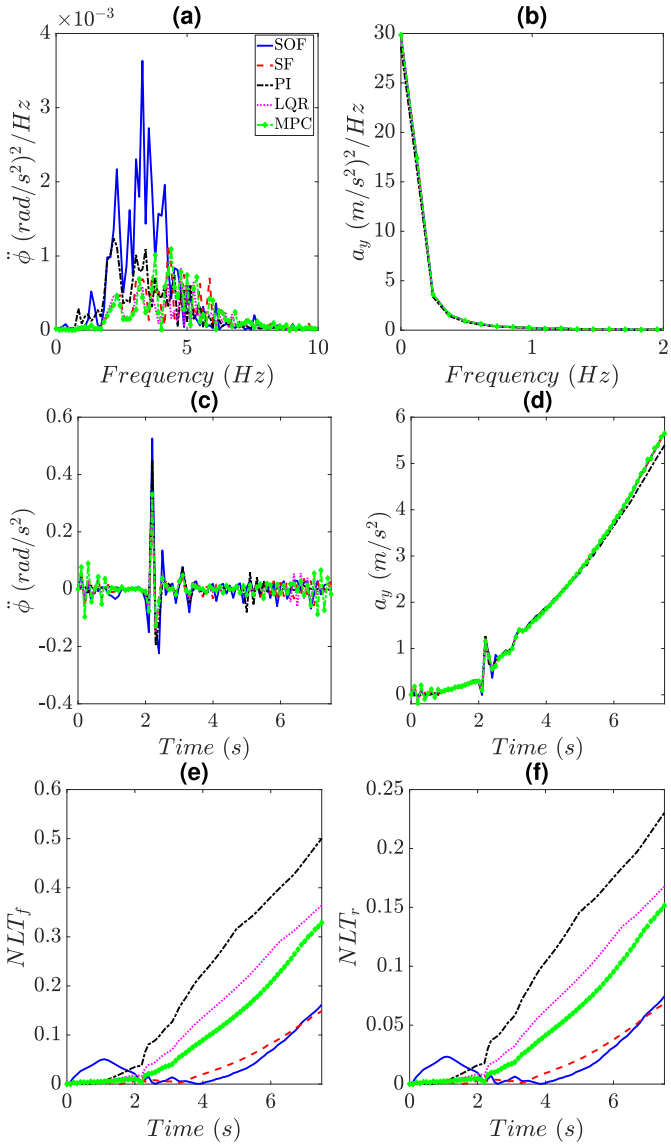

Fig. 10. Vehicle behavior obtained with a J-turn maneuver and an increasing vehicle speed profile. (a) Roll acceleration PSD, (b) Lateral acceleration PSD, (c) Roll acceleration, (d) Lateral acceleration, (e) NLT of the front axle, (f) NLT of the rear axle.

full-state information is not required for SOF control, there is no significant performance difference between the proposed SOF and SF controllers. Indeed, the maximum NLT and the lateral error only vary around 10%. Hence, the control performance is not severely affected with the proposed SOF control method even if some specific sensors are removed for cost reasons.

From the results of the three above test scenarios, we can see that the proposed event-triggered SOF controller allows achieving the best overall vehicle path tracking control performance. This is mainly due to the following main reasons.

- The roll stability, the communication delay and the asynchronous phenomenon caused by the sampling process were not considered for the PI control design.
- Although the same vehicle model (5) was used for SOF, LQR and MPC designs, the effect of external disturbances was not explicitly taken into account in the design of LQR and MPC controllers.

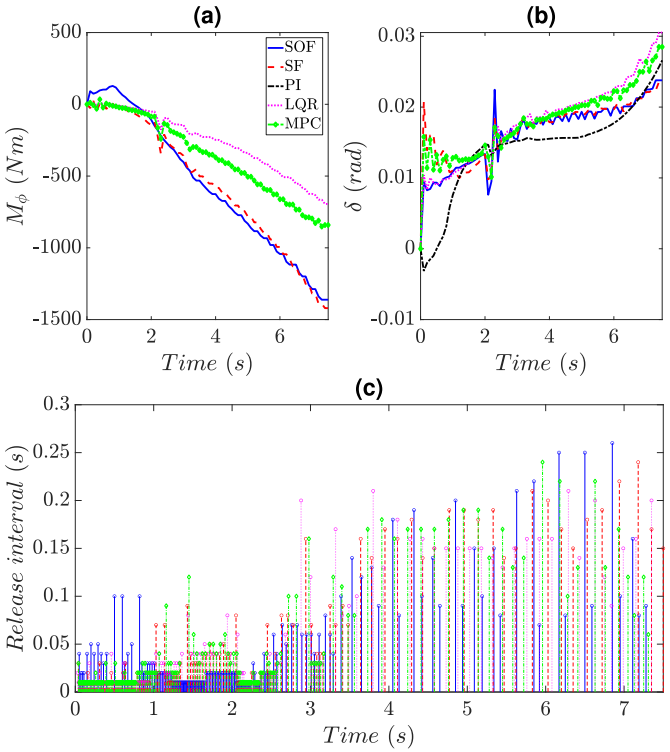

Fig. 11. Control performance obtained with a J-turn maneuver and an increasing vehicle speed profile. (a) Anti-roll moment, (b) Steering angle, (c) Event-triggering instants.

Furthermore, the proposed SOF controller does not require full-state information, *i.e.*, the knowledge of the sideslip angle β and the roll angle ϕ is not necessary for control implementation, as the case of SF, LQR and MPC controllers. This is particularly appealing for practical uses since high-cost sensors and/or additional observers can be avoided. These advantages of the proposed SOF control method clearly confirm the contributions of the paper.

V. Conclusion

A new event-triggered SOF control method has been proposed for path tracking autonomous vehicles, taking into account the roll dynamics and network-induced delays. Using a polytopic control framework, the time-varying vehicle speed and the transmission errors due to network delays are explicitly taken into account in the control design. The vehicle closed-loop control performance under the effects of transmission errors, network-induced delays and external disturbances is guaranteed via Lyapunov-Krasovskii stability theory. Moreover, an LMI-based iterative procedure has been proposed to search for a suboptimal SOF control solution. The control performance has been evaluated with a high-fidelity vehicle model in CarSim software under different test scenarios. A comparative study with respect to related path tracking control methods in the literature has been performed to highlight the effectiveness of the proposed event-triggered SOF controller. The simulation results clearly show that the proposed controller enhances the ride comfort by reducing the roll acceleration frequency components over time. The roll stability is increased, as the NLT index is reduced 50% during the most severe test scenario. Moreover, the obtained results also confirm that the proposed event-triggering mechanism can improve the efficiency of the vehicle control network system in terms of data exchange, as it discards around 64% of the computed control orders. To evaluate the real-time control performance, experimental tests are planned for future works with a real vehicle platform on a real test track in our labs [22], [38]. Moreover, the proposed event-triggered SOF control scheme can be further extended to take into account the modeling uncertainties in lateral tires forces and/or the actuator faults.

References

[1] R. Xiong, L. Li, C. Zhang, K. Ma, X. Yi, and H. Zeng, "Path tracking of a four-wheel independently driven skid steer robotic vehicle through a cascaded NTSM-PID control method," *IEEE Trans. Instrum. Meas.*, vol. 71, pp. 1–11, 2022.

[2] X. Zhou, Z. Wang, H. Shen, and J. Wang, "Robust adaptive path-tracking control of autonomous ground vehicles with considerations of steering system backlash," *IEEE Trans. Intell. Vehicles*, vol. 7, no. 2, pp. 315–325, Jun. 2022.

[3] P. Li, A.-T. Nguyen, H. Du, Y. Wang, and H. Zhang, "Polytopic LPV approaches for intelligent automotive systems: State of the art and future challenges," *Mech. Syst. Signal Process.*, vol. 161, Dec. 2021, Art. no. 107931.

[4] Y. He, X. Yan, X. Lu, D. Chu, and C. Wu, "Rollover risk assessment and automated control for heavy duty vehicles based on vehicle-to-infrastructure information," *IET Intell. Transp. Syst.*, vol. 13, no. 6, pp. 1001–1010, Jun. 2019.

[5] X. Qian, C. Wang, and W. Zhao, "Rollover prevention and path following control of integrated steering and braking systems," *Proc. Inst. Mech. Eng., D, J. Automobile Eng.*, vol. 234, no. 6, pp. 1644–1659, May 2020.

[6] T. Xu and X. Wang, "Roll stability and path tracking control strategy considering driver in the loop," *IEEE Access*, vol. 9, pp. 46210–46222, 2021.

[7] A.-T. Nguyen, P. Chevrel, and F. Claveau, "LPV static output feedback for constrained direct tilt control of narrow tilting vehicles," *IEEE Trans. Control Syst. Technol.*, vol. 28, no. 2, pp. 661–670, Mar. 2020.

[8] A. Dandiwala, B. Chakraborty, D. Chakravarty, and J. Sindha, "Vehicle dynamics and active rollover stability control of an electric narrow three-wheeled vehicle: A review and concern towards improvement," *Veh. Syst. Dyn.*, vol. 61, no. 2, pp. 399–422, 2022.

[9] R. Hajiloo, A. Khajepour, A. Kasaiezadeh, S.-K. Chen, and B. Litkouhi, "Integrated lateral and roll stability control of multi-actuated vehicles using prioritization model predictive control," *IEEE Trans. Veh. Technol.*, vol. 71, no. 8, pp. 8318–8329, Aug. 2022.

[10] T. A. Nguyen, "Preventing the rollover phenomenon of the vehicle by using the hydraulic stabilizer bar controlled by a two-input fuzzy controller," *IEEE Access*, vol. 9, pp. 129168–129177, 2021.

[11] F. Viadero-Monasterio, B. Boada, M.-J. Boada, and V. Díaz, "H_∞ dynamic output feedback control for a networked control active suspension system under actuator faults," *Mech. Syst. Signal Process.*, vol. 162, Jan. 2022, Art. no. 108050.

[12] N. A. I. Ruslan, N. H. Amer, K. Hudha, Z. A. Kadir, S. A. F. M. Ishak, and S. M. F. S. Dardin, "Modelling and control strategies in path tracking control for autonomous tracked vehicles: A review of state of the art and challenges," *J. Terramechanics*, vol. 105, pp. 67–79, Feb. 2023.

[13] X. Li, C. Liu, B. Chen, and J. Jiang, "Robust adaptive learning-based path tracking control of autonomous vehicles under uncertain driving environments," *IEEE Trans. Intell. Transp. Syst.*, vol. 23, no. 11, pp. 20798–20809, Nov. 2022.

[14] X. Zhou, Z. Wang, and J. Wang, "Popov-H_∞ robust path-tracking control of autonomous ground vehicles with consideration of sector bounded kinematic nonlinearity," *J. Dyn. Syst., Meas., Control*, vol. 143, Jun. 2021, Art. no. 111004.

[15] H. Zhang, X. Zhang, and J. Wang, "Robust gain-scheduling energy-to-peak control of vehicle lateral dynamics stabilisation," *Vehicle Syst. Dyn.*, vol. 52, no. 3, pp. 309–340, Mar. 2014.

[16] E. Alcala, V. Puig, J. Quevedo, T. Escobet, and R. Comasolivas, "Autonomous vehicle control using a kinematic Lyapunov-based technique with LQR-LMI tuning," *Control Eng. Pract.*, vol. 73, pp. 1–12, Apr. 2018.

[17] Y. Tian, Q. Yao, C. Wang, S. Wang, J. Liu, and Q. Wang, "Switched model predictive controller for path tracking of autonomous vehicle considering rollover stability," *Veh. Syst. Dyn.*, vol. 60, no. 12, pp. 4166–4185, 2021.

[18] F. Lin, S. Wang, Y. Zhao, and Y. Cai, "Research on autonomous vehicle path tracking control considering roll stability," *Proc. Inst. Mech. Eng., D, J. Automobile Eng.*, vol. 235, no. 1, pp. 199–210, Jan. 2021.

[19] D. Hrovat, S. Di Cairano, H. E. Tseng, and I. V. Kolmanovsky, "The development of model predictive control in automotive industry: A survey," in *Proc. IEEE Int. Conf. Control Appl.*, Dubrovnik, Croatia, Oct. 2012, pp. 295–302.

[20] Y. Chen, Y. Zhang, and F. Zhang, "Personalized path generation and robust H_∞ output-feedback path following control for automated vehicles considering driving styles," *IET Intell. Transp. Syst.*, vol. 15, no. 12, pp. 1582–1595, Dec. 2021.

[21] C. M. Ho, C. H. Nguyen, and K. K. Ahn, "Adaptive fuzzy observer control for half-car active suspension systems with prescribed performance and actuator fault," *Electronics*, vol. 11, no. 11, p. 1733, May 2022.

[22] B. Boada, F. Viadero-Monasterio, H. Zhang, and M.-J. Boada, "Simultaneous estimation of vehicle sideslip and roll angles using an integral-based event-triggered H_∞ observer considering intravehicle communications," *IEEE Trans. Veh. Technol.*, vol. 72, no. 4, pp. 4411–4425, Apr. 2023.

[23] C. Young, J. Zambreno, H. Olufowobi, and G. Bloom, "Survey of automotive controller area network intrusion detection systems," *IEEE Des. Test.*, vol. 36, no. 6, pp. 48–55, Dec. 2019.

[24] Z. Luan, J. Zhang, W. Zhao, and C. Wang, "Trajectory tracking control of autonomous vehicle with random network delay," *IEEE Trans. Veh. Technol.*, vol. 69, no. 8, pp. 8140–8150, Aug. 2020.

[25] R. Wang, H. Jing, C. Hu, F. Yan, and N. Chen, "Robust H_∞ path following control for autonomous ground vehicles with delay and data dropout," *IEEE Trans. Intell. Transp. Syst.*, vol. 17, no. 7, pp. 2042–2050, Jul. 2016.

[26] J. Zhao, W. Li, C. Hu, G. Guo, Z. Xie, and P. K. Wong, "Robust gain-scheduling path following control of autonomous vehicles considering stochastic network-induced delay," *IEEE Trans. Intell. Transp. Syst.*, vol. 23, no. 12, pp. 23324–23333, Dec. 2022.

[27] F. Viadero-Monasterio, B. L. Boada, H. Zhang, and M. J. L. Boada, "Integral-based event triggering actuator fault-tolerant control for an active suspension system under a networked communication scheme," *IEEE Trans. Veh. Technol.*, early access, May 26, 2023, doi: 10.1109/TVT.2023.3279460.

[28] Z. Wu, J. Sun, and S. Hong, "RBFNN-based adaptive event-triggered control for heterogeneous vehicle platoon consensus," *IEEE Trans. Intell. Transp. Syst.*, vol. 23, no. 10, pp. 18761–18773, Oct. 2022.

[29] H. Li, L. Zhang, X. Zhang, and J. Yu, "A switched integral-based event-triggered control of uncertain nonlinear time-delay system with actuator saturation," *IEEE Trans. Cybern.*, vol. 52, no. 11, pp. 11335–11347, Nov. 2022.

[30] W. Li, H. Du, D. Ning, W. Li, S. Sun, and J. Wei, "Event-triggered H_∞ control for active seat suspension systems based on relaxed conditions for stability," *Mech. Syst. Signal Process.*, vol. 149, Feb. 2021, Art. no. 107210.

[31] Z. Ye, D. Zhang, Z.-G. Wu, and H. Yan, "A3C-based intelligent event-triggering control of networked nonlinear unmanned marine vehicles subject to hybrid attacks," *IEEE Trans. Intell. Transp. Syst.*, vol. 23, no. 8, pp. 12921–12934, Aug. 2022.

[32] X. Ge, I. Ahmad, Q.-L. Han, J. Wang, and X.-M. Zhang, "Dynamic event-triggered scheduling and control for vehicle active suspension over controller area network," *Mech. Syst. Signal Process.*, vol. 152, May 2021, Art. no. 107481.

[33] H. Zhang, X. Zheng, H. Li, Z. Wang, and H. Yan, "Active suspension system control with decentralized event-triggered scheme," *IEEE Trans. Ind. Electron.*, vol. 67, no. 12, pp. 10798–10808, Dec. 2020.

[34] M.-J. Boada, B. Boada, and H. Zhang, "Event-triggering H_∞-based observer combined with NN for simultaneous estimation of vehicle sideslip and roll angles with network-induced delays," *Nonlinear Dyn.*, vol. 103, no. 3, pp. 2733–2752, 2021.

[35] A.-T. Nguyen, J. Rath, T.-M. Guerra, R. Palhares, and H. Zhang, "Robust set-invariance based fuzzy output tracking control for vehicle autonomous driving under uncertain lateral forces and steering constraints," *IEEE Trans. Intell. Transp. Syst.*, vol. 22, no. 9, pp. 5849–5860, Sep. 2021.

[36] D. Kapsalis, O. Sename, V. Milanes, and J. J. Molina, "A reduced LPV polytopic look-ahead steering controller for autonomous vehicles," *Control Eng. Pract.*, vol. 129, Dec. 2022, Art. no. 105360.

[37] J. Wang, M. Dai, G. Yin, and N. Chen, "Output-feedback robust control for vehicle path tracking considering different human drivers' characteristics," *Mechatronics*, vol. 50, pp. 402–412, Apr. 2018.

[38] C. M. Nguyen, A.-T. Nguyen, and S. Delprat, "Neural-network-based fuzzy observer with data-driven uncertainty identification for vehicle dynamics estimation under extreme driving conditions: Theory and experimental results," *IEEE Trans. Veh. Technol.*, vol. 72, no. 2, pp. 8686–8696, Jul. 2023.

[39] A.-T. Nguyen, C. Sentouh, and J.-C. Popieul, "Driver-automation cooperative approach for shared steering control under multiple system constraints: Design and experiments," *IEEE Trans. Ind. Electron.*, vol. 64, no. 5, pp. 3819–3830, May 2017.

[40] J. P. Redondo, B. L. Boada, and V. Díaz, "LMI-based H_∞ controller of vehicle roll stability control systems with input and output delays," *Sensors*, vol. 21, no. 23, p. 7850, Nov. 2021.

[41] P. H. S. Coutinho, M. L. C. Peixoto, M. Bernal, A.-T. Nguyen, and R. M. Palhares, "Local sampled-data gain-scheduling control of quasi-LPV systems," *IFAC-PapersOnLine*, vol. 54, no. 4, pp. 86–91, 2021.

[42] K. Tanaka and H. Wang, *Fuzzy Control Systems Design and Analysis: A Linear Matrix Inequality Approach*. Hoboken, NJ, USA: Wiley, 2004.

[43] A. Seuret and F. Gouaisbaut, "Wirtinger-based integral inequality: Application to time-delay systems," *Automatica*, vol. 49, no. 9, pp. 2860–2866, Sep. 2013.

[44] P. Park, J. W. Ko, and C. Jeong, "Reciprocally convex approach to stability of systems with time-varying delays," *Automatica*, vol. 47, no. 1, pp. 235–238, Jan. 2011.

[45] A. H. K. Palmeira, J. M. Gomes da Silva, and J. V. Flores, "Regional stabilization of nonlinear sampled-data control systems: A quasi-LPV approach," *Eur. J. Control*, vol. 59, pp. 301–312, May 2021.

[46] M. Meléndez-Useros, M. Jiménez-Salas, F. Viadero-Monasterio, and B. L. Boada, "Tire slip H_∞ control for optimal braking depending on road condition," *Sensors*, vol. 23, no. 3, p. 1417, Jan. 2023.

[47] C. Agulhari, R. Oliveira, and P. Peres, "LMI relaxations for reduced-order robust H_∞ control of continuous-time uncertain linear systems," *IEEE Trans. Autom. Control*, vol. 57, no. 6, pp. 1532–1537, Jun. 2012.

[48] J. Lofberg, "YALMIP: A toolbox for modeling and optimization in MATLAB," in *Proc. IEEE Int. Conf. Robot. Autom.*, Sep. 2004, pp. 284–289.

[49] C. F. Caruntu, M. Lazar, R. H. Gielen, P. P. J. van den Bosch, and S. Di Cairano, "Lyapunov based predictive control of vehicle drivetrains over CAN," *Control Eng. Pract.*, vol. 21, no. 12, pp. 1884–1898, Dec. 2013.

[50] C. Liang, X. Xu, F. Wang, S. Wang, and Z. Zhou, "CAN-induced asynchronous random delays-considered mode transition system for DM-PHEV based on constrained output feedback robust control strategy," *IEEE Trans. Veh. Technol.*, vol. 71, no. 6, pp. 5995–6006, Jun. 2022.

[51] G. Wang, M. Chadli, H. Chen, and Z. Zhou, "Event-triggered control for active vehicle suspension systems with network-induced delays," *J. Franklin Inst.*, vol. 356, no. 1, pp. 147–172, Jan. 2019.

[52] M. Doumiati, A. Victorino, A. Charara, and D. Lechner, "Lateral load transfer and normal forces estimation for vehicle safety: Experimental test," *Vehicle Syst. Dyn.*, vol. 47, no. 12, pp. 1511–1533, Dec. 2009.

[53] Z. Wan and M. V. Kothare, "An efficient off-line formulation of robust model predictive control using linear matrix inequalities," *Automatica*, vol. 39, no. 5, pp. 837–846, May 2003.

Fernando Viadero-Monasterio received the B.S. degree in industrial engineering from Universidad de Cantabria (UNICAN), Santander, Spain, in 2018, and the M.S. degree in industrial engineering and the Ph.D. degree in mechanical engineering from University Carlos III de Madrid (UC3M), Madrid, Spain, in 2020 and 2023, respectively. He joined the Department of Mechanical Engineering, UC3M, in 2018. His current research interests include vehicle dynamics, vehicle safety, control systems, fault-tolerant control, and non-linear systems. He is a member of the IFToMM Technical Committee for Transportation Machinery.

Anh-Tu Nguyen (Senior Member, IEEE) received the degree in engineering and the M.Sc. degree in automatic control from the Grenoble Institute of Technology, Grenoble, France, in 2009, and the Ph.D. degree in automatic control from the University of Valenciennes, Valenciennes, in 2013. He is currently an Associate Professor with the INSA Hauts-de-France, Université Polytechnique Hauts-de-France, Valenciennes. His current research interests include robust control and estimation, cybernetics control systems, and human–machine shared control, with a strong emphasis on mechatronics applications. He is an Associate Editor of IEEE TRANSACTIONS ON INTELLIGENT TRANSPORTATION SYSTEMS, *Control Engineering Practice* (IFAC Journal), *The Journal of Engineering* (IET), *SAE International Journal of Vehicle Dynamics, Stability, and NVH*, *Automotive Innovation* (Springer), and *Frontiers in Control Engineering*. He is the guest editor for special issues in various international journals.

Jimmy Lauber received the M.S., Ph.D., and H.D.R. degrees in automatic control from the University of Valenciennes, Valenciennes, France, in 2000, 2003, and 2011, respectively. Since 2014, he has been a Full Professor with the CNRS Laboratory, LAMIH UMR 8201, Polytechnic University of Hauts-de-France, Famars, France. His current research interests include nonlinear and fuzzy control/observation and their applications to sustainable transport (powertrain control and autonomous train), human mobility, and rehabilitation (walking analysis and assistive devices).

Maria Jesus L. Boada received the degree in industrial engineering and the Ph.D. degree in industrial technologies from University Carlos III de Madrid (UC3M), Madrid, Spain, in 1996 and 2002, respectively. From 1997 to 2002, she was a Research and Teaching Assistant with the Department of Systems and Automation Engineering, UC3M. In 2002, she joined the Department of Mechanical Engineering, UC3M. Since 2020, she has been a Full Professor and co-responsible with the Research Group Advanced Vehicle Dynamics and Mechatronic Systems (VEDYMEC). Her current research interests include artificial neural networks, control systems, Kalman filters, system dynamics modeling, sensor fusion, vehicle safety, advanced vehicle dynamics, MR dampers, and bus structures.

Beatriz L. Boada received the Industrial Engineering and Ph.D. degrees from Universidad Carlos III de Madrid (UC3M), Madrid, Spain, in 1996 and 2002, respectively. From 1997 to 2002, she was a Research Assistant with the Department of Systems and Automation Engineering, UC3M. She was with localization and mapping problems in the field of robotics. She is currently a Full Professor with the Mechanical Engineering Department, UC3M. Since 2017, she has been co-responsible with the Research Group Research Group Advanced Vehicle Dynamics and Mechatronic Systems (VEDYMEC). Her current research interests include intelligent vehicles both autonomous and motorized, control of vehicles in vertical, lateral dynamics, magnetorheological dampers, uncertainty modeling, and the estimation of mechanical systems.